JOURNAL OF PROPULSION AND POWER
Vol. 23, No. 1, January–February 2007

Combined Numerical and Experimental Investigation of a Hobby-Scale Pulsejet

T. Geng,* A. Kiker Jr.,* R. Ordon,* A. V. Kuznetsov,† T. F. Zeng,‡ and W. L. Roberts§
North Carolina State University, Raleigh, North Carolina 27695-7910

DOI: 10.2514/1.18593

The pulsejet, due to its simplicity, may be an ideal micropropulsion system, but has received very little attention since the mid 1950s. Here, modern computational and experimental tools are used to investigate the operation of a hobby-scale (50 cm overall length) pulsejet. Gas dynamics, acoustics, and chemical kinetics are all involved and are studied to gain an understanding of the various physical phenomena affecting pulsejet operation, scalability, and efficiency. A Bailey Machining Service hobby pulsejet is instrumented to obtain pressure, temperature, thrust, and frequency. CH* chemiluminescence is used to determine the combustion time and high-speed imaging of the reed valve operation is undertaken to determine the valve duty cycle. Laser Doppler velocimetry is used to measure the instantaneous exhaust velocity in these unsteady combustion devices. Numerical simulations are performed using CFX to model the 3-D compressible viscous flow in the pulsejet using the integrated Westbrook–Dryer single-step combustion model. The turbulent flow and reaction rate are modeled with the k–ε model and the eddy dissipation model, respectively. Simulation results provide physical insight into the pulsejet cycle; comparisons with experimental data obtained in this research are carried out. The traditional view of a pulsejet as a 1/4 wave tube operating on the Humphrey cycle is modified to account for valve operation and finite chemical kinetics.

Nomenclature

Da	=	Damköhler number, $t_{\text{flow}}/t_{\text{chem}}$
k	=	turbulence kinetic energy per unit mass
L	=	pulsejet length
P_k	=	shear production of turbulence
Pr_t	=	turbulent Prandtl number
p'	=	modified pressure in k–ε model
R_k	=	reaction rate
S_E	=	energy source
t_{flow}	=	fluid timescale, k/ε
t_{chem}	=	chemical timescale
v'_{KI}	=	stoichiometric coefficient for reactant I in reaction K
v''_{KI}	=	stoichiometric coefficient for product I in reaction K
W_I	=	molecular weight of species I
ε	=	turbulence dissipation rate
λ	=	thermal conductivity
μ_{eff}	=	total viscosity
μ_t	=	turbulence viscosity

I. Introduction

THE pulsejet is perhaps one of the simplest propulsion devices, with passively moving reed valves being the only moving parts. The pulsejet has been described as a 1/4 wave tube, and clearly acoustics play an important role in its operation. The pulsejet is based on the Humphrey thermodynamic cycle, where isochoric heat addition (combustion) follows an isentropic compression and isobaric heat rejection follows an isentropic expansion. However, because the wave compression is weak, the thermodynamic efficiency is low, especially compared with the Brayton cycle where mechanical compression offers very high thermodynamic efficiency. To optimize and determine the scalability of these propulsion devices, a better understanding of the interaction between the acoustics, fluid mechanics, and chemical kinetics is needed.

The concept of a pulsejet can be tracked back to the beginning of the 20th century. Two French engineers, Esnault and Peltrie, patented a design of an engine that drove a turbine wheel [1]. The Esnault–Peltrie design was based on the principle of two opposing pulsating combustion columns fitted in a single straight tube. In the 1930s, the German engineer Paul Schmidt designed the first working pulsejet, which was called the Schmidt tube [2,3]. The first practical application of the pulsejet was the German Vergeltungswaffe-1 (V-1) weapon (also known as the "buzz bomb" due to the low-frequency acoustic emission) in World War II. It was a pilotless flying bomb, which can be viewed as a prototype of a modern cruise missile.

Reynst [2], best known for his "combustion pot" discovery, believed that pulsejet engines operate on an acoustic resonating principle analogous to that of a 1/4 wave organ pipe. Reynst related the pressures and velocities in a characteristic Schmidt tube cycle to standing wave theory for small amplitude oscillations (i.e., by using linear acoustics). In a collection of works edited by Weinberg, Zinn [4] gives a very thorough development of pressure oscillations in a closed tube driven by linear heat addition (i.e., amplitudes of oscillation and heat addition are small). Zinn suggests that the Esnault–Peltrie analysis can be easily adjusted for the 1/4 wave structure of a pulsejet simply by substituting the fundamental mode approximation for that of a tube open at one end and closed at the other. In theory, such a solution would determine the characteristics of the oscillations inside the engine and the range of operating conditions for which pulsating operation is possible.

Towards the later part of the second half of the century, interest in pulsejet applications quietly subsided. The continuing improvement of the turbojet (Brayton cycle) engine clearly gave it advantages as a propulsion system for atmospheric flight (higher thermodynamic efficiency, supersonic flight speeds, throttleability, etc.) over unsteady combustion technology [5]. Most of these research efforts before the turbojet's insurgence were pushed to the side and slowly forgotten amid the progress of technology. Pulsejets continued to be pursued by hobbyists for RC aircraft and boat propulsion. A very comprehensive review of hobby-scale pulsejets is given by Boradin

Presented as Paper 4378 at the 41st AIAA/ASME/SAE/ASEE Joint Propulsion Conference & Exhibit, Tucson, AZ, 10–13 July 2005; received 7 July 2005; accepted for publication 27 May 2006; revision received 6 July 2006.

*Graduate Student, Department of Mechanical & Aerospace Engineering. Member AIAA.
†Associate Professor, Department of Mechanical & Aerospace Engineering.
‡Assistant Professor, Department of Mechanical & Aerospace Engineering.
§Professor, Department of Mechanical & Aerospace Engineering. Senior Member AIAA.

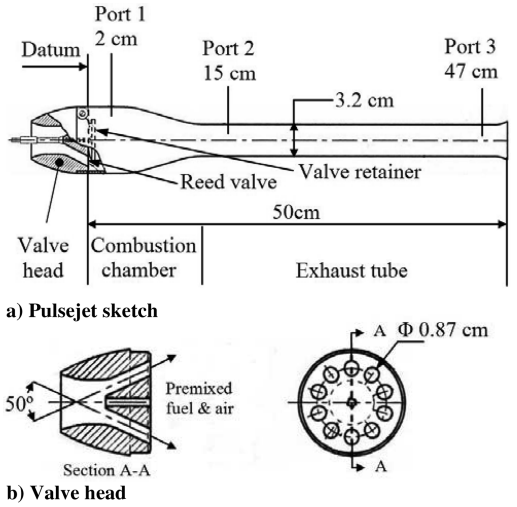

Fig. 1 BMS pulsejet geometry and dimensions.

[6]; unfortunately, it has not been translated from Russian into English as of yet.

The pulsejet is an unsteady propulsion device that generates intermittent thrust. However, because the wave compression is weak, the thermodynamic efficiency is low, especially compared with the Brayton cycle where mechanical compression offers very high thermodynamic efficiency. This lack of thermodynamic efficiency is somewhat offset by the fundamental simplicity of the pulsejet. Although various designs were proposed after the first Schmidt tube, the basic design remains the same, and is shown in Fig. 1. The reactants enter the tube when the pressure in the combustion chamber is lower than ambient pressure. Residual hot gases and heat transfer from the hot walls raise the reactant temperature above the autoignition temperature, initiating ignition and combustion of the reactants. The ensuing heat release increases the pressure, and these hot gases then expand down the exhaust duct and exit at high velocity, generating thrust. The hot gases at the exit have expanded to nearly atmospheric pressure and their momentum causes an expansion wave to propagate back up the exhaust duct towards the combustion chamber. When the expansion wave hits the reed valves, the subatmospheric pressure causes the valves to open, and fresh reactants are pulled into the combustion chamber, equalizing the pressure and closing the reed valves. The cycle then repeats itself.

In the $1/4$ wave tube analysis (open at one end and closed at the other), the introduction of mass while the valves are open is neglected. In fact, when the valves are open, the resonant frequency corresponds to a $1/2$ wave tube (open at both ends). Clearly, the $1/4$ tube analysis cannot capture this. The thermodynamic cycle is also more complex than the Humphrey cycle because the combustion occurs neither isochorically nor isobarrically, but somewhere in between, with the pressure rise in the combustion chamber being a competition between heat release rate (dictated by the chemical kinetics) and pressure release through expansion of products down the exhaust duct. Therefore, a more sophisticated computational model, validated by experimental measurements, is necessary to capture all the relevant physics.

The major advantage of a pulsejet is its simplicity. No mechanical compressor is needed to produce a pressure rise in the combustion chamber. However, early research has shown that pulsejets have low overall efficiency, which caused the termination of this line of research until recently, when it was found that thermodynamic efficiency of conventional engines (such as gas turbines) decreases nonlinearly with decreasing the characteristic engine scale. Pulsejets are especially attractive as candidates for miniaturization due to their simple design.

The pulsejet investigated in this research is an off-the-shelf Bailey Machining Service (BMS) pulsejet used by hobbyists for RC aircraft and boat propulsion. As shown in Fig. 1, the BMS pulsejet consists of three sections: the valve head, the combustion chamber, and the exhaust duct. It has the total length of 50 cm (in this paper, the total length is defined as the length from the combustion chamber to the exit of the exhaust tube). Air and fuel are premixed in the valve head and enter the combustion chamber through reed valves. The reed valves are open when the pressure in the combustion chamber is lower than the ambient pressure and closed otherwise. A spark plug is used to ignite the air-fuel mixture. After several combustion events, the fuel and air mixture is ignited by the contact with the hot wall and the residual hot products in the pulsejet. Thus, the spark plug is only required to initiate the combustion during the first few cycles.

The aim of the current research is to develop a detailed understanding of the chemical kinetic, fluid mechanic, and acoustic processes occurring within the pulsejet. An experimentally validated CFD model will allow the optimization of the pulsejet and help determine its suitability for miniaturization.

II. Preliminary Analysis of the Pulsejet Operation Cycle

One of the most distinct characteristics of the pulsejet is the ominous sound (i.e., $120+$ dB) caused by the combustion events that happen hundreds of times per second (for the hobby-scale pulsejet). A wave diagram is shown in Fig. 2 and illustrates the primary waves in the pulsejet. The ordinate spans from 0 to L, which corresponds to the inlet and the outlet of the jet, respectively. The abscissa can be treated as a nondimensional time for one cycle. In each cycle, valves are first closed and a constant-volume (ideally) heat addition (combustion) generates compression waves simultaneously: a compression wave a traveling downstream and a compression wave b traveling upstream. The compression wave a is reflected as a strong expansion wave a_1 by the outlet of the jet. Because the opening of the reed valves is neglected, the left end of the pulsejet is modeled as an impermeable wall. The initial compression wave b is reflected as a compression wave b_1. When the wave b_1 reaches the pulsejet exit, it is reflected as an expansion wave b_2. The expansion wave a_1 propagates upstream and when it enters the combustion chamber, the resulting subatmospheric pressure causes the reed valves to open and fresh reactants are pulled into the combustion chamber. The expansion wave is reflected as an expansion wave at $x = 0$, and propagates down the exhaust tube, reflecting as a compression wave. When the compression wave enters the combustion chamber, the reactants are consumed, and the cycle repeats itself. As seen in this diagram, the primary acoustic wave propagates through the duct four times, hence the reason for analyzing this device as a $1/4$ wave tube.

The actual events are obviously more complex than those shown in Fig. 2. The opening of the valves and ensuing mass addition cannot be neglected. Because of geometric variations in the combustion

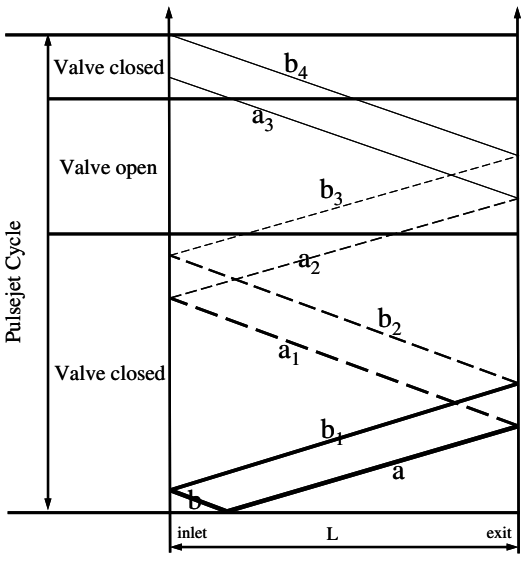

Fig. 2 Wave diagram for valved pulsejet operation.

chamber, there are a series of reflected waves traveling up and down the tube. The interactions between these waves make the analysis of the pulsejet operation extremely complex. Numerical simulation makes it possible to monitor different waves propagating in this system.

III. Experimental Setup

Fuel flow rates are measured with a rotameter for gaseous fuels and by mass balance for the liquid fuels. The data presented here are with liquid ethanol fuel. The liquid ethanol is pulled into the air flow in the venturi and vaporizes as it flows past the open reed valves and into the combustion chamber. Much difficulty was found in getting the pulsejet to run on gaseous propane due primarily to the destruction of the reed valves by the high-temperature combustion process. The evaporation of the liquid ethanol aided in cooling the reed valves, and this cooling effect was absent with the gaseous propane, resulting in excessive heating and valve failure. The jet is attached to a low friction bearing assembly for thrust measurements. To measure instantaneous thrust, a Kistler piezoelectric force sensor combined with a Kistler charge amplifier was used. This load cell requires a preload, which was attained by securing the bearing shuttle with bungee cords to the test stand. To measure the instantaneous static pressure, Omega DPX101-250 high-speed pressure transducers were used in conjunction with an Agilent oscilloscope. Type-B thermocouples were used to measure average gas temperature inside the jet at various axial locations. To determine the location and characteristic times associated with the oxidation of the hydrocarbon fuel, a system of lenses, fiber optic cable, a filter, and a photo multiplier tube were used to detect the intermediate combustion radical, CH^*. Instantaneous jet exit velocities were also measured using standard single component Laser Doppler velocimetry (LDV), from which thrust could be calculated and compared with the measured thrust and used to validate the computational model.

Several jet configurations based on the BMS pulsejet were used in this research. The total length of the standard configuration is 50 cm. The exhaust tube is 3.2 cm in diameter but flares to 3.8 cm at the exit. There are ten 0.87-cm-diam holes on the valve head through which the air/fuel mixture enters the tube. Three ports were welded on to the pulsejet along the jet axis for diagnostic measurements. The port locations can be seen in Fig. 1, where Ports 1, 2, and 3 are 2, 15, and 47 cm from the beginning of the combustion chamber, respectively. Temperature, pressure, and CH^* data were taken at each port (the latter two simultaneously). Additional tail pipe extensions were manufactured so that the jet could be lengthened in 7.5 cm increments to determine the relationship between the exhaust duct length and engine operation.

IV. Numerical Model

A. Model Geometry and Mesh Description

The computational domain has exactly the same geometry and dimension as the BMS jet. For simplicity, the reed valves and the valve retainer were not modeled. The function of the reed valve was modeled by supplying an equation relating the inflow velocity (V_{inflow}) and the pressure difference across the valve. This equation, obtained from experimental measurements in the actual pulsejet venturi-reed valve assembly, is

$$V_{\text{inflow}} = \begin{Bmatrix} \frac{3(P_0-P_1)}{1000}\frac{[\text{m/s}]}{[P_a]}, & P_1 < P_0 \\ 0, & P_1 > P_0 \end{Bmatrix} \tag{1}$$

where P_1 is the pressure immediately after the reed valve and P_0 is the ambient pressure. The inflow velocity has a 25 deg radially outward trajectory, similar to that observed in the experiments. The flow in the pulsejet is assumed to be axially symmetric; therefore, the computational domain is only 1/10 of the actual pulsejet, or 36 deg in the θ-direction.

B. Numerical Model and Governing Equations

The current study models unsteady, three-dimensional, compressible, viscous flow with heat transfer and radiation. The CFX5.7 software package is used.[‖] The second-order transient scheme and high-resolution advection scheme are used to capture the compression/expansion waves. The timestep is chosen such that the Courant number is unity and the solution has a convergence criterion of 10^{-4} in residual mean square value.

The computations are performed on the NC State IBM Blade center using a single 3.0 GHz Intel Xeon processor. Typical computational time for one cycle of the pulsejet is 20 CPU hours. The turbulent flow is modeled using a k–ε model based on the Reynolds-averaged Navier–Stokes (RANS) equations. The viscous effect in the boundary layer region is modeled by the log-law, in which the empirical formulas are provided to connect the wall conditions to the dependent variables at the near-wall mesh node.

1. *Model of Turbulent Flow and Heat Transfer*

Governing equations for the fluid flow are given next. The continuity equation is

$$\frac{\partial \rho}{\partial t} + \nabla \cdot (\rho \boldsymbol{U}) = 0 \tag{2}$$

The momentum equation based on the eddy viscosity assumption is given by

$$\frac{\partial \rho \boldsymbol{U}}{\partial t} + \nabla \cdot (\rho \boldsymbol{U} \otimes \boldsymbol{U}) = \nabla p' + \nabla \cdot \{\mu_{\text{eff}}[\nabla \boldsymbol{U} + (\nabla \boldsymbol{U})^T]\} \tag{3}$$

where μ_{eff} is the total viscosity that accounts for turbulent viscosity, and p' is the modified pressure given by

$$p' = p + \frac{2}{3}\rho k \tag{4}$$

The k–ε model is based on the eddy viscosity concept, which assumes

$$\mu_{\text{eff}} = \mu + \mu_t \tag{5}$$

where μ_t is the turbulent viscosity:

$$\mu_t = C_\mu \rho \frac{k^2}{\varepsilon} \tag{6}$$

The k–ε model includes the following equations for the kinetic energy k and the dissipation rate of turbulence ε:

$$\frac{\partial(\rho k)}{\partial t} + \nabla \cdot (\rho \boldsymbol{U} k) = \nabla \cdot \left[\left(\mu + \frac{\mu_t}{\sigma_k}\right)\nabla k\right] + P_k - \rho\varepsilon \tag{7}$$

$$\frac{\partial(\rho \varepsilon)}{\partial t} + \nabla \cdot (\rho \boldsymbol{U} \varepsilon) = \nabla \cdot \left[\left(\mu + \frac{\mu_t}{\sigma_\varepsilon}\right)\nabla \varepsilon\right] + \frac{\varepsilon}{k}(C_{\varepsilon 1 k} - C_{\varepsilon 2}\rho\varepsilon) \tag{8}$$

where $C_{\varepsilon 1}$, $C_{\varepsilon 2}$, σ_k, and σ_ε are model constants (their values are given in Table 1) and P_k is the turbulence production due to the viscous force:

$$P_k = \mu_t \nabla \boldsymbol{U} \cdot (\nabla \boldsymbol{U} + \nabla \boldsymbol{U}^T) - \frac{2}{3}\nabla \cdot \boldsymbol{U}(3\mu_t \nabla \cdot \boldsymbol{U} + \rho k) \tag{9}$$

The energy equation is

$$\frac{\partial \rho(h + \frac{1}{2}\boldsymbol{U}^2 + k)}{\partial t} - \frac{\partial P}{\partial t} + \nabla \cdot \left[\rho \boldsymbol{U}\left(h + \frac{1}{2}\boldsymbol{U}^2 + k\right)\right.$$
$$= \nabla \cdot \left(\lambda \nabla T + \frac{\mu_t}{Pr_t}\nabla h\right) + S_E \tag{10}$$

[‖]Data available on-line at http://www.ansys.com/products/cfx.asp [cited 1 May 2006].

Table 1 Constants used in CFX computational code

Symbol	Description	Dimensions	Value
A	Eddy dissipation model coefficient	1	4.0
B	Eddy dissipation model coefficient	1	0.5
$C_{\varepsilon 1}$	k–ε turbulence model constant	1	1.44
$C_{\varepsilon 2}$	k–ε turbulence model constant	1	1.92
σ_k	Turbulent model constant for the k equation	1	1.0
σ_ε	k–ε turbulence model constant	1	1.3
C_μ	k–ε turbulence model constant	1	0.09

2. Eddy Dissipation Model for Combustion

The model assumes complete vaporization and mixing producing homogeneous premixed reactants at an overall stoichiometric ratio of unity. The eddy dissipation model (EDM) is used to simulate the unsteady combustion process [7,8]. The only reaction products are CO_2 and H_2O. The EDM assumes that either reaction is fast compared to turbulent mixing (high Damköhler number), or the reaction rate is proportional to the timescale of turbulent mixing. The timescale of turbulent mixing, which depends on the eddy properties, is determined as the ratio of k and ε.

The reaction rate is determined from the minimum of expressions (11) and (12):

$$R_k = A\frac{\varepsilon}{k}\min\left(\frac{[I]}{v'_{\mathrm{KI}}}\right) \tag{11}$$

$$R_k = AB\frac{\varepsilon}{k}\left(\frac{\sum_P [I]W_I}{\sum_P W_I v''_{\mathrm{KI}}}\right) \tag{12}$$

where $[I]$ is the molar concentration of the reactant I and P loops over all product components. A and B are model constants and their values are given in Table 1. The autoignition and flame quenching process are modeled with two parameters: chemical timescale and extinction temperature. In this case, chemical timescale is 0.0004 s and extinction temperature is 800 K. Autoignition happens when the chemical timescale is smaller than the local turbulence timescale and the local temperature is higher than the extinction temperature. The turbulence timescale is calculated from the flowfield as k/ε. Similarly, the flame is locally quenched whenever the temperature is less than the specified extinction temperature, or the chemical timescale is larger than the turbulence timescale. This extinction temperature was chosen based on experimental measurements of pressure and oscillation frequency.

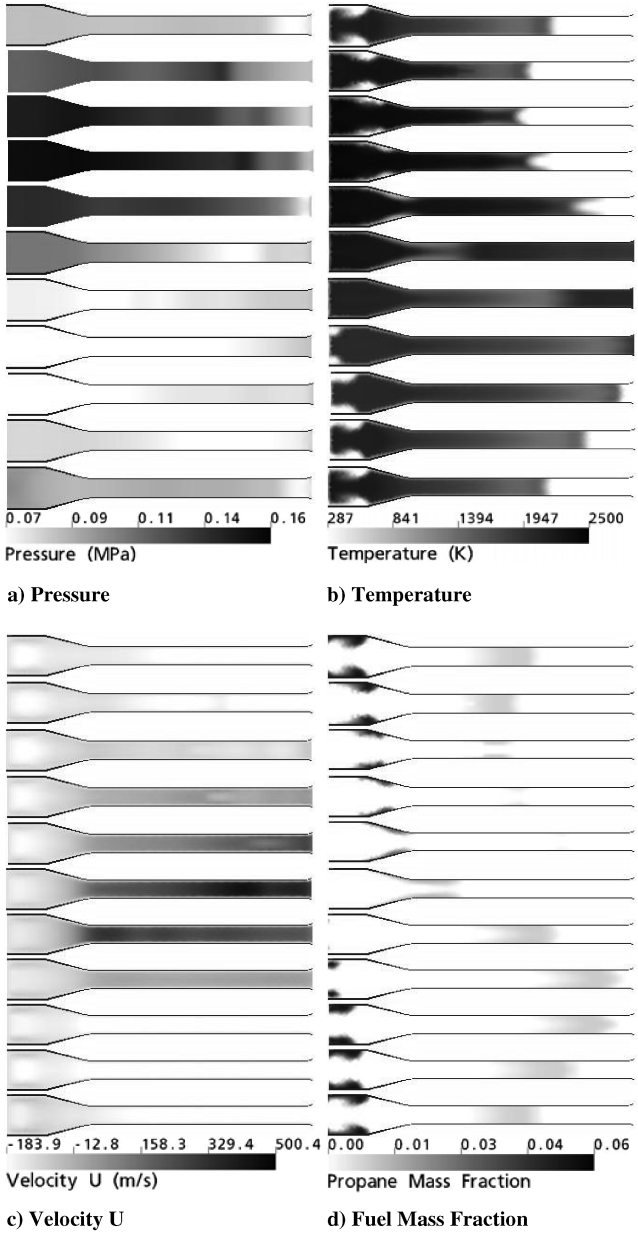

a) Pressure **b) Temperature**

c) Velocity U **d) Fuel Mass Fraction**

Fig. 3 Simulation results of the pulsejet cycle.

V. Results and Discussion

Figure 3 shows an example of the simulation results for the BMS pulsejet. The pulsejet is static and the wall temperature is 300 K. The pressure outside the pulsejet is atmospheric. The stoichiometric fuel/air mixture enters the combustion chamber with the velocity described by Eq. (1). The pressure, temperature, axial velocity u, and fuel mass fraction on the cross section of the pulsejet for one cycle are shown in Figs. 3a–3d.

The general pulsejet cycle can be illustrated as the following. The combustion event occurs when the combustion chamber pressure is above atmospheric and the temperature of the fuel/air mixture increases, due to mixing with residual products, to the autoignition temperature. A compression wave is generated and increases temperature and pressure in the combustion chamber, driving the flow toward the exit at gradually increasing velocity. When the compression wave reaches the pulsejet exit, expansion waves are generated due to overexpansion and travel back to the combustion chamber. Flow velocity reaches its positive maximum near the exit. The expansion wave decreases the pressure in the tube and the combustion chamber to subatmosphere and backflow occurs at the exit. When the combustion chamber pressure is below atmospheric, reed valves open up and let the next charge of fuel/air mixture into the chamber. This mass addition, along with the backflow, increases the combustion chamber pressure. When the pressure in the combustion chamber approaches the atmosphere pressure, the next cycle begins.

The first five steps in Fig. 3 can be treated as the filling process, whereas the second five steps are the burning process. Reaction occurs at the beginning of the burning process. Most of the combustion chamber is filled with the reactants during the filling cycle. This confirms that the drop of temperature at port 1 is caused by cold reactants. The fuel/air mixture is injected towards the wall and generates a strong vortex behind the valve. This enhances turbulence in this region and increases the reaction rate as well because the reaction rate, according to EDM, is proportional to the turbulence intensity. It is found that during the fuel burning process, there is a small amount of fuel along the wall in the transition region that does not burn. This is not expected because experiments indicate that the wall temperature in this region is always high enough to ignite the fuel. A possible reason is that in the wall region, the turbulence timescale is very small due to the small turbulence kinetic energy. If this small turbulence timescale is smaller than the chemical timescale, the flame extinction in that region is enabled in the simulation model. Further work is needed to investigate the influence of the chemical timescale.

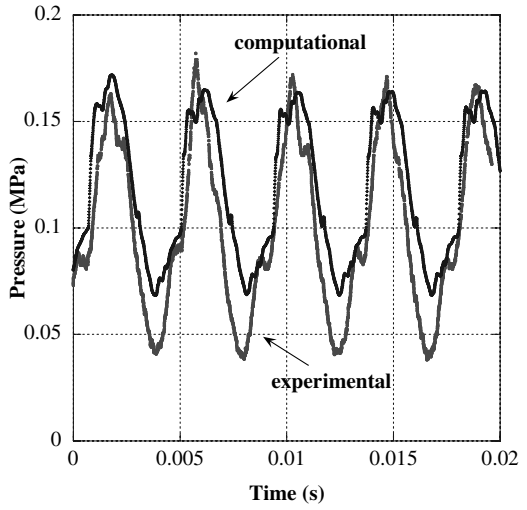

a) Port 1

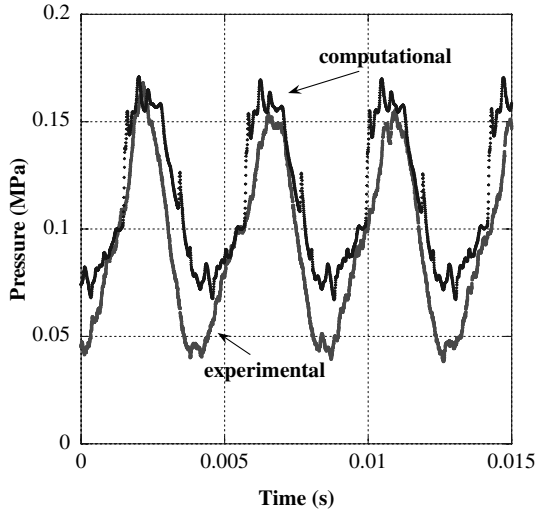

b) Port 2

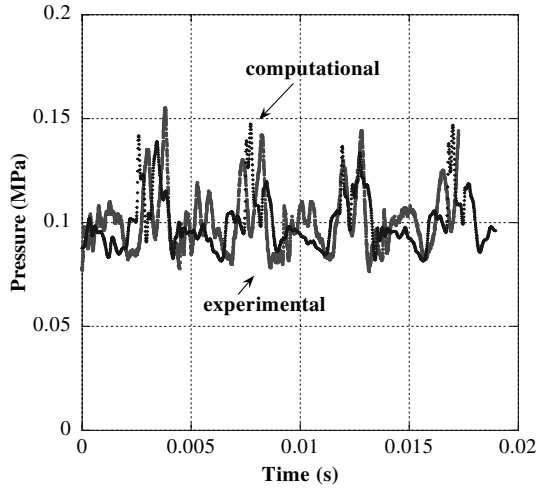

c) Port 3

Fig. 4 Instantaneous pressure, both measured and calculated.

Figures 4a–4c show the experimental and computational pressure vs time at three ports. The measured frequency is 232 Hz, with a fluctuation of approximately 10 Hz, whereas the computed frequency is 242 Hz; this is a very good agreement. To compare structure, the time scales have been stretched so that the experimental and computational oscillations coincide. The peak pressure in the combustion chamber (port 1) is calculated to be 0.17 MPa, in very good agreement with the experimental measurements. The model is

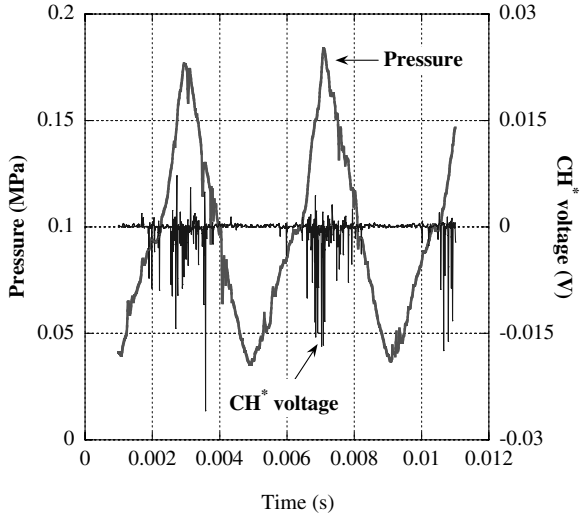

Fig. 5 CH* chemiluminescence measurements and experimental combustion chamber pressure.

also able to replicate the small pressure blip on the rising part of the oscillation, most likely due to acoustic wave reflections. The model does not do as well in predicting the negative pressures measured in the combustion chamber, where the measurements are considerably more negative. Recall that the valves are not being modeled, so it is not surprising that the model does a relatively poor job at predicting the minimum pressures. The total fuel flow rate is the same in both the computations and the experiments, however. In Fig. 4c, a complex exhausting process is observed both computationally and experimentally, with multiple reflections occurring at the jet exit. The code does a remarkably good job at predicting these multiple reflections.

By drawing a line at the ambient pressure (0.1 MPa), it is evident that each cycle consists of a high-pressure portion and a low-pressure (subatmospheric) portion. The positive and negative peaks are approximately equal in magnitude; however, the upper portion is always slightly larger. This happens because the flow is nearly fully expanded at the exit and reflected expansion waves have an approximately same strength as the compression waves (see Fig. 2, waves a and a_1). The small difference between the peaks is primarily caused by the inflow of reactants, valve losses, and viscous losses. The strength and the number of reflected expansion waves are important to the pulsejet operation because they create the necessary subatmospheric condition in the combustion chamber. This phase of the engine's cycle must be sufficiently long in duration to permit sufficient reactants to enter the combustion chamber to initiate the next cycle.

During a cycle of operation, the pulsejet is constantly changing its acoustic characteristics. For example, while the valves are open, the acoustic wave perceives the tube as a $1/2$-wave tube with pressure release surfaces seen at either end. Yet, while the valves are closed, the jet behaves as a $1/4$-wave tube where a solid wall boundary replaces the pressure release surface at the front end. However, due to the change in the cross section area, the jet behaves more like a $1/6$-wave tube, which is indicated by the frequency data. This is so because the area change results in complex wave interactions in the pulsejet. The operation frequency is also affected by the temperature inside the pulsejet, which determines the local speed of sound.

To see when this pressure rise is occurring as compared to the combustion, CH* at port 1 was measured, and the result is shown in Fig. 5. CH* is a short-lived intermediate combustion radical appearing only in an active reaction zone. The measurements were made by setting up lenses attached to a fiberoptic cable to capture the light emitted from port 1. The emission was transmitted through a 430 nm (the wavelength emitted by CH*) filter and measured by a photomultiplier tube (PMT) attached to an oscilloscope. It was found that the pressure peaks resulting from reflected waves coincide with the peak combustion pressure events to attain resonance. These

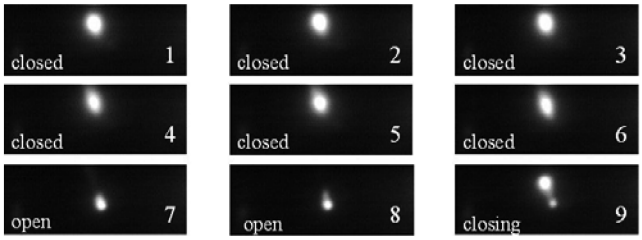

Fig. 6 The open/close duty cycle for the reed valves.

results suggest that chemical times (responsible for controlling fluid dynamic times) must be similar to acoustic times to assure dependency. From Fig. 5 it is evident that combustion occurs mostly during the superatmospheric portion of the cycle. The subatmospheric portion, when fresh reactants are introduced, shows no CH^*, and therefore no combustion. A finite amount of time is required for the residual hot products to mix with the fresh reactants and raise their temperature to the autoignition temperature. This information is used in the EDM simulations to model the flame extinction.

The duty cycle of the reed valves (i.e., the duration they spend open during each cycle) was also measured, and these results are presented in Fig. 6. A He-Ne laser and high-speed camera were used to make these measurements. The laser was used to "paint" a spot on the valve to make use of the camera's limited light sensitivity at high speed. The painted spot was observed to move when the valves were open due to their deflection. The camera acquired images at 2 kHz while the jet operated at 230 Hz, so there were a little over 9 frames acquired per cycle. After looking over many cycles, the results were then averaged and it was concluded that the valves remained open for approximately 30% of the cycle duration. This information was used to validate the inlet boundary conditions in the computation model, where the valve operation was simplified. The duration for the premixed reactants to enter the combustion chamber should be approximately 30% of the cycle duration.

The pulsejet thrust was measured experimentally, both instantaneous and mean, and computed. Figure 7 shows the measured instantaneous thrust and the simultaneously measured pressure at port 2. The mean thrust was measured to be 25 N by compressing a spring with known spring constant. As observed in Fig. 7, the thrust oscillates at the same frequency as the pressure, but is 180 deg out of phase as expected because the pulsejet trades the high static pressure for the high exhaust velocity. The negative thrust is caused by the backflow. To increase thrust, the backflow can be reduced; the frequency and the mixing rate can be increased. Of these options, the reduction of backflow is most challenging because the backflow is related to many factors such as the pressure rise and pulsejet length. The simulated thrust is plotted with experimental result for thrust and shown in Fig. 8. The frequency is the same, as expected, and the model is predicting the complex double peak structure observed in the measurements. However, the magnitude is

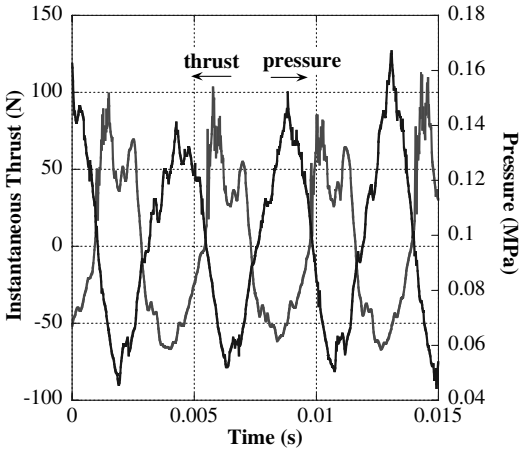

Fig. 7 Instantaneous thrust and port 2 pressure measurements.

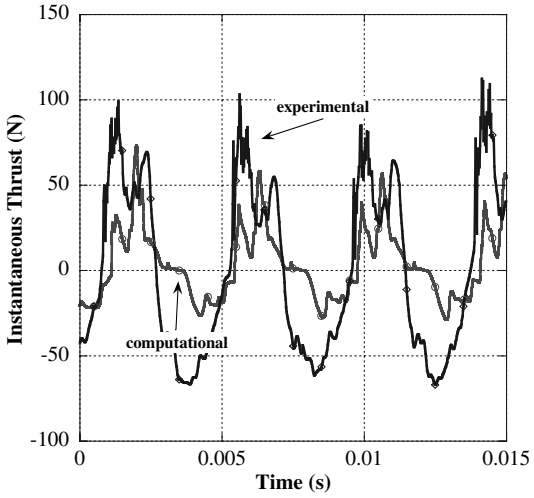

Fig. 8 Instantaneous thrust comparison between measurement and calculation.

not well predicted. One possible reason for this is the wall temperature for the simulation may lower than the experiments, which would result in a loss of enthalpy.

The exit velocity was also measured using a single component LDV setup operating in a forward scattering mode. A curve fit of the experimental data clearly shows a sinusoidal behavior, with a frequency of 235 Hz, and is shown in Fig. 9. There is a strong negative component of velocity during a part of the cycle. This confirms the negative thrust predicted and measured in this pulsejet. To our knowledge, this is the first time a negative velocity in the pulsejet has been reported.

Figure 10 shows the temperature data at the three ports. Because of the finite size of the thermocouple bead, instantaneous temperature measurements were not possible and only cycle-averaged temperatures are shown. Computational results show that port 1 has the highest peak temperature whereas port 2 has the highest mean temperature. The majority of the combustion process is occurring near port 1, and thus the peak temperature occurs at this location. The mean temperature (both measured and calculated) is lower at port 1 due to the cold reactants being introduced during each cycle. As seen in the simulation results at port 2, the cold reactants do not penetrate this far upstream before reacting, thus the mean temperature is much closer to the peak temperature at this location. The peak temperature is lower at port 2 than port 1 due to heat losses to the walls (which is included in the model). Port 3 has the lowest temperature due to both expansion of the hot gases and heat loss to the wall. It is also clear from the temperature simulations that the ambient air is entrained into the exhaust duct during a portion of the cycle. The cycle-averaged computational temperatures are compared with the measured mean temperatures. At port 1, the calculated temperature of 1900 K is 50 K higher than the measured mean temperature of 1850 K, whereas at port 2, the calculations overpredict the temperature by 130 K, and underpredict the temperature at port 3 by 60 K. Recall that the thermocouple measurements are not radiation corrected, having the greatest effect on port 2 which has the highest mean temperature. The computational model assumes that the environment is always at 300 K, so the ambient air that is entrained during the negative exit velocity portion of the cycle artificially depresses the mean cycle-averaged temperature because the hot gas from the jet increases the outside air temperature, and this is neglected in the model.

The peak temperatures in ports 1 and 2 are coincident in time, indicating multiple ignition sites and nearly homogeneous burning of reactants in the combustion chamber. The peak temperature at port 3 is delayed in time relative to ports 1 and 2 due to the finite propagation time of the hot products. More details of each temperature profile are given in Figs. 11–13.

Figure 11 shows an expanded view of the temperature profile at port 1, just behind one of the valves. Features such as the introduction

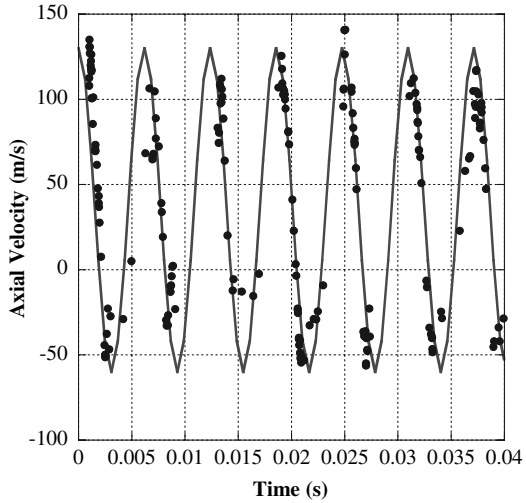

Fig. 9 Measured exit velocity via LDV with 235 Hz sine wave curve fit.

of fresh reactants, their warming up to the autoignition temperature, their reaction and resulting heat release, and then their cooling due to expansion converting this thermal enthalpy into kinetic energy (and thus thrust) are all readily apparent.

In Fig. 12, it is shown that the temperature does not change a great deal during the cycle. The hot gases provide the thermal energy necessary to ignite the subsequent reactant charge. The temperature difference will be due to a combination of kinetic energy generation and heat losses through the walls, which is being modeled.

Figure 13 shows the temperature time history near the exit plane. The pressure is very dynamic at the exit due to interactions of the acoustic waves and material waves with the ambient surroundings. The material wave (fluid mechanic wave) makes one round trip during a complete cycle. One trip is for the compression waves traveling from combustion chamber to the exit and the other is for expansion waves traveling back to the combustion chamber. The acoustic wave makes two round trips during the same cycle. The presence of the acoustic wave is clearly seen in the temperature profile, showing up as local maxima. The model is also accurately predicting the negative velocity during the refraction wave portion of the cycle, as evidenced by the very low temperatures in the exit duct. This corresponds to ambient air being pulled into the exit duct; the ambient air is always at 300 K. The expansion of the hot gases leaving the exhaust duct is not modeled. It is evident that there will be some expansion waves at the exit because the gases are underexpanded. Thus, the fluid which is pulled into the exhaust duct will contain some warm products; however, it is not believed to have a major effect on pulsejet operation.

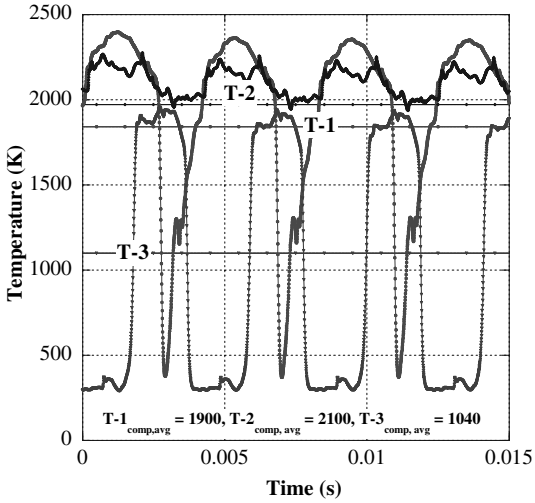

Fig. 10 Calculated temperature at three axial locations, with comparison to measured (mean) temperatures.

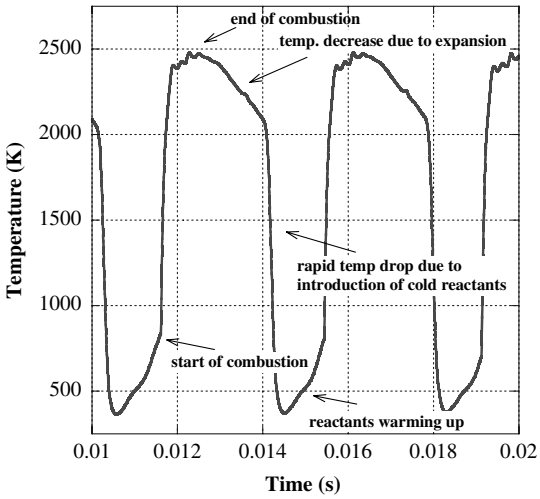

Fig. 11 Details of calculated temperature at port 1 (just behind 12 valves).

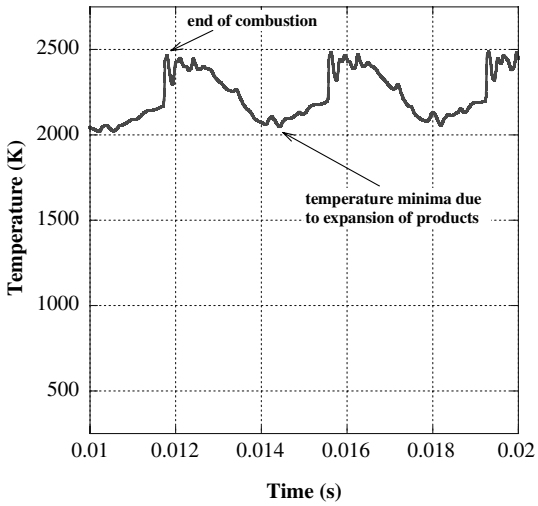

Fig. 12 Details of calculated temperature at port 2 (end of combustion section).

As stated, to obtain higher thrust, it is desirable to have high operation frequency and mixture ratio. For a fixed size of the combustion chamber and fixed mixture ratio, changing the operation frequency can be accomplished by varying the jet length. The

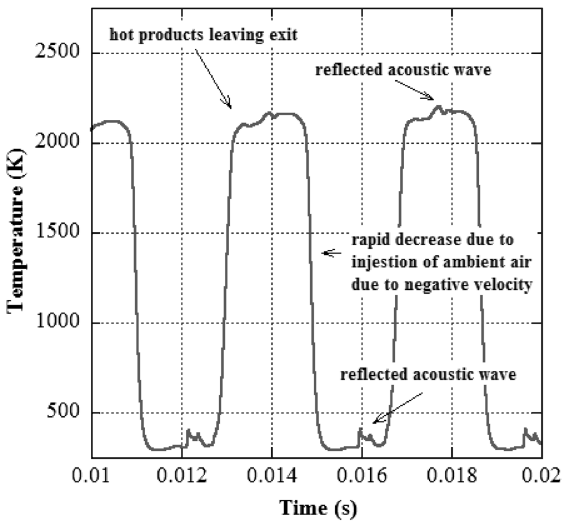

Fig. 13 Details of calculated temperature at port 3 (near the exit plane).

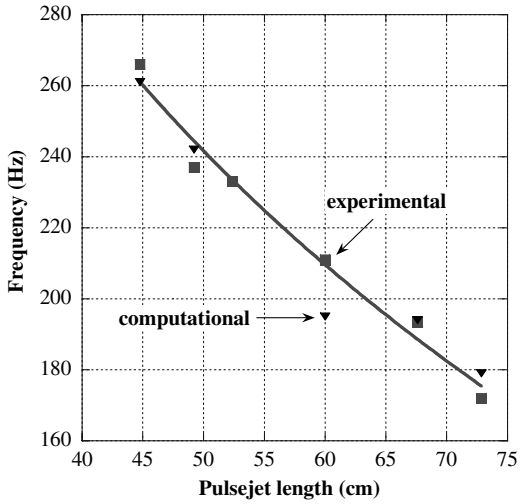

Fig. 14 Effect of pulsejet length on frequency, both experimental and calculated.

relation between the jet length and the operation frequency, obtained both experimentally and computationally, with good agreement between the two, is shown in Fig. 14. The solid line in Fig. 14 represents a $1/L$ curve fit.

VI. Conclusions

A better understanding of the pulsejet as a propulsion device has been achieved through a coupled experimental/computational study of a hobby-scale pulsejet. This 50 cm valved pulsejet produced an average thrust of 25 N and operating frequency of 240 Hz when running on ethanol. The measured exit velocity, via LDV, behaves like a 235 Hz sinusoidal wave, with a significant negative velocity component. A He-Ne laser and high-speed camera were used to examine the duty cycle of the reed valves, and used as an input for the computations, and reveals that the valves remained open for approximately 30% of the cycle duration. CH^* was measured to determine the location and temporal extent and characteristics of the combustion event. Combined with simultaneous combustion chamber pressure measurements, it is evident that combustion happens in during the superatmosphere portion of the cycle. The experimentally validated simulation model shows that the reflected expansion waves create the necessary subatmospheric condition in the combustion chamber, the strength and the number of these waves are important to the pulsejet operation. The duration of the low-pressure phase of the engine's cycle must be sufficiently long to permit sufficient reactants to enter the combustion chamber to initiate the next cycle. The analysis of peak temperatures in different axial positions indicates multiple ignition sites and nearly homogeneous burning of reactants in the combustion chamber. The simulation also shows the location and size of the vortex in the combustion chamber generated by the injection of the fuel/air mixture, which increases the reaction rate because the reaction rate is proportional to the turbulence intensity. The acoustic model for the 50 cm valved pulsejet is a function of many factors such as valve duty cycle, temperature, combustion chamber volume, and total length. Acoustically, the pulsejet can be modeled as a $1/6$-wave tube, and this new model is verified by both the experimental and computational results.

Acknowledgments

This project is sponsored by the Defense Advanced Research Projects Agency (DARPA) under the supervision of R L. Rosenfeld, Grant No. HR0011-0-1-0036. The content of the information does not necessarily reflect the position or policy of the Government and no official endorsement should be inferred. The authors would also like to thank Vincent Castelli for his helpful comments and suggestions.

References

[1] Foa, J. V., *Elements of Flight Propulsion*, Wiley, New York, 1960.
[2] Reynst, F. H., "Pulsating Firing for Steam Generators," *Pulsating Combustion*, edited by M. W. Thring, Pergamon, New York, 1961.
[3] Tsien, H. (ed.), *Jet Propulsion*, Guggenheim Aero. Lab., Pasadena, CA, 1946, pp. 21–59.
[4] Zinn, B. T., *In Advanced Combustion Methods*, edited by F. J. Weinberg, Academic Press, Inc., London, 1986, pp. 113–81.
[5] Shepherd, D. G., *Aerospace Propulsion*, Elsevier, New York, 1972.
[6] Boradin, V., *Pulse Air Jet Engines for Flying Plane Models*, DOSAAF, Moscow, 1958, in Russian.
[7] Poinsot, T., and Veynante, D., *Theoretical and Numerical Combustion*, R. T. Edwards, Philadelphia, 2001.
[8] Pope, S. B., *Turbulent Flows*, Cambridge Univ. Press, Cambridge, England, U.K., 2000.

A. Gupta
Associate Editor